Complex Nanoparticle of Light-Emitting MEH-PPV with Au: Enhanced Luminescence

Mi Suk Kim,[†] Dong Hyuk Park,[†] Eun Hei Cho,[†] Kyoung Ho Kim,[†] Q-Han Park,[†] Hugeun Song,[‡] Dae-Chul Kim,[‡] Jeongyong Kim,[‡] and Jinsoo Joo[†,*]

[†]Department of Physics, Korea University, Seoul 136-713, Korea, and [‡]Department of Physics, University of Incheon, Incheon 402-749, Korea

ABSTRACT Complex nanoparticles (NPs) of poly(2-methoxy-5-(2′-ethylhexyloxy)-*p*-phenylene vinylene) (MEH-PPV) NP adsorbed with Au NPs (MEH-PPV/Au NPs) were fabricated through a reprecipitation method. The formation of MEH-PPV/Au NP complexes was confirmed through high-resolution transmission electron microscopy and Fourier transform infrared experiments. The laser confocal microscope photoluminescence (PL) efficiency of the complex MEH-PPV/Au single NP dramatically increased compared with that of the MEH-PPV single NP without Au NPs, which was directly confirmed through color charge-coupled device images. The enhanced PL efficiency of the MEH-PPV/Au NP complex might have originated from the energy transfer effect in a surface plasmon resonance coupling between a MEH-PPV NP and Au NPs. The strong local field enhancement due to nanogaps between Au NPs in the background of a light-emitting MEH-PPV NP might be another origin of the PL enhancement of the NP complex, as supported by finite difference time domain calculations. We also observed the blue shift of the PL peaks of the single MEH-PPV and MEH-PPV/Au NP, compared with the solution PL peaks of those NPs.

KEYWORDS: nanoparticle · MEH-PPV · Au · photoluminescence · surface plasmon

Organic and inorganic nanoparticles (NPs) having metallic, semiconducting, and/or magnetic properties have been fabricated through various synthetic methods[1,2] and applied to biosensors and chemical sensors,[3,4] optoelectronic devices,[5,6] and nanodevices.[7,8] The intrinsic characteristics of a group of NPs have mainly been studied in terms of their ensemble average with a form of homogeneously dispersed solution or an array of NPs. For example, the luminescence color of semiconducting NPs in solution can vary with the size of the NPs because of the variation of the energy band gap.[9,10] Recently, the self- and directed-assembly mechanisms (including external electrostatic or magnetic forces) required for NPs to be transformed into desired nanostructures have been studied.[11] Also, various functionalized hybrid nanostructures using NPs, such as hybrid NPs of semiconductor/metal,[12] hybrid core−shell NPs of metal/polymer or ferromagnet/silica,[13,14] and complex nanocomposites of semiconducting NP/π-conjugated polymers,[15] have been studied for the enhancement of their intrinsic properties and/or the development of desired functions for applications. These hybrid or complex nanostructures have many applications in bioengineering,[16] diagnostic sensing,[17] surface-enhanced Raman spectroscopy (SERS),[18] near-field microscopy,[5] and holographic structures.[19] However, the optical properties of a single unit of NPs (*i.e.*, an isolated single NP) have not been thoroughly investigated.

Hybrid or complex nanostructures of organic semiconductors with inorganic metals such as Au, Ag, Ni, and Pt have been applied to photoluminescence (PL) enhancement and DNA sensing through a surface plasmon resonance (SPR) coupling.[20−26] When the surface plasmon (SP) energy of nanoscale metals is closely matched with the photon energy of light-emitting organic semiconductors, the resulting resonance (the so-called SPR) can lead to an energy transfer between the nanoscale materials, resulting in enhanced PL. A local electromagnetic (EM) field enhancement in a form of metal-based nanobow tie or nanohole (*i.e.*, metal-based nanoscale gap) has recently been studied in the field of photonics,[27,28] which might also contribute to the tuning luminescence efficiency and/or color of organic-based hybrid or complex nanostructures.

Herein, we report on the fabrication and nanoscale luminescent characteristics of an isolated single unit of complex NPs consisting of light-emitting poly(2-methoxy-5-(2′-ethylhexyloxy)-*p*-phenylene vinylene) (MEH-PPV) NP adsorbed with Au NPs (MEH-PPV/Au NP). The nanostructure of the MEH-PPV/Au NP complex was confirmed through analysis using high-resolution transmission electron microscopy (HR-TEM) and Fourier transform infrared (FTIR) experiments. The nanoscale

*Address correspondence to jjoo@korea.ac.kr.

Received for review January 18, 2009 and accepted May 18, 2009.

Published online May 20, 2009.
10.1021/nn900071w CCC: $40.75

luminescent characteristics of a MEH-PPV/Au single NP were compared to those of a MEH-PPV single NP using a laser confocal microscope (LCM) with a high spatial resolution. We observed considerable enhancement of LCM PL intensity for the MEH-PPV/Au single NP compared to that of the MEH-PPV single NP without adsorption of Au NPs. The enhanced PL of the MEH-PPV/Au NP complex might have originated from the energy transfer effect in

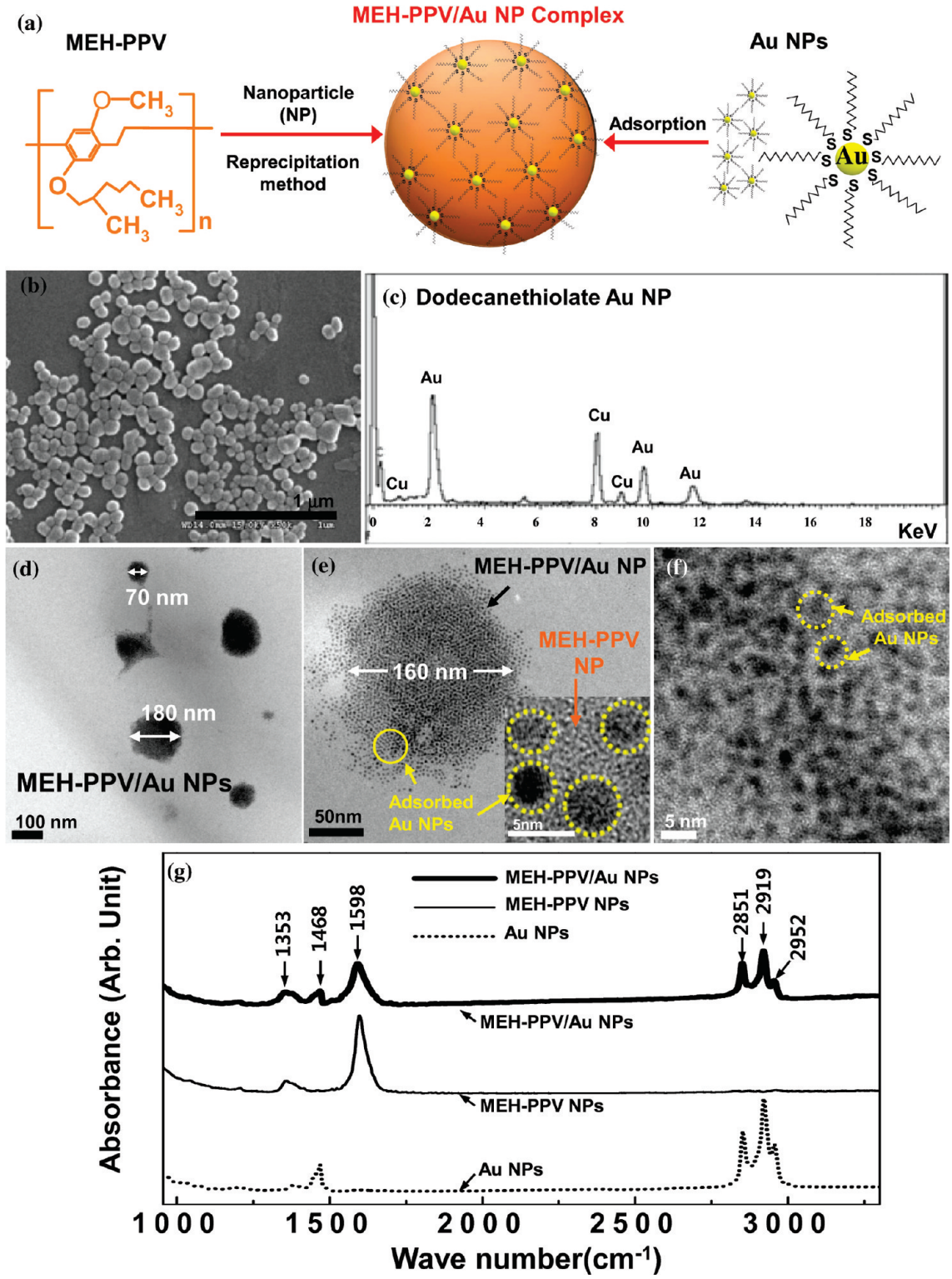

Figure 1. (a) Schematic diagram of the preparation of MEH-PPV/Au NP. (b) SEM image of MEH-PPV NPs. (c) EDS spectrum in HR-TEM experiments for the dodecanethiolate Au NPs. (d,e) HR-TEM images of MEH-PPV/Au NPs complexes. Inset of (e): Magnification of HR-TEM image of the MEH-PPV/Au single NP. The dotted circles represent the Au NPs. (f) Another magnification of HR-TEM image of MEH-PPV/Au NP complex. (g) FTIR spectra of the Au NPs (dotted curve), MEH-PPV NPs (solid curve), and MEH-PPV/Au NPs (solid bold curve).

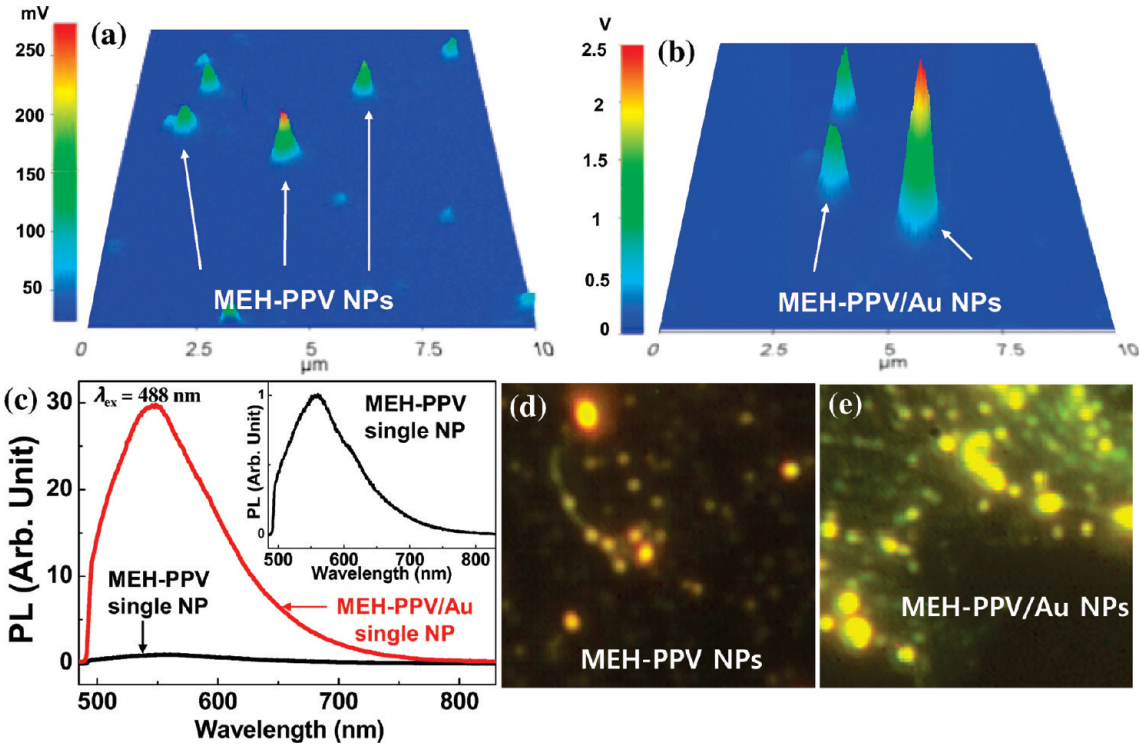

Figure 2. Three-dimensional LCM PL images of the (a) MEH-PPV NPs and (b) MEH-PPV/Au NPs. The color scale bars in the left-hand side represent the intensity of LCM PL. (c) Comparison of LCM PL spectra of the MEH-PPV single NP (black curve) and MEH-PPV/Au single NP (red curve). Inset: Magnification of LCM PL spectrum of MEH-PPV single NP for a reference. Color CCD images of the (d) MEH-PPV NPs and (e) MEH-PPV/Au NPs.

the SPR coupling between the MEH-PPV NP and Au NPs and/or from a local EM field enhancement of nanogaps between Au NPs in the background of a light-emitting MEH-PPV NP. We also observed that the PL spectrum of the MEH-PPV/Au single NP was blue-shifted compared with that of the ensemble average of the NPs dispersed in a solution.

RESULTS AND DISCUSSION

Figure 1a shows a schematic diagram of a MEH-PPV/Au NP complex. The dodecanethiolate Au NPs were adsorbed in a MEH-PPV single NP. MEH-PPV NPs as a mother NP were prepared using a reprecipitation method.[29] Figure 1b shows an SEM image of the MEH-PPV NPs. The diameters of the MEH-PPV NPs were about 40−150 nm from the SEM image. The dodecanethiolate Au NPs with a diameter of 2−4 nm as a daughter NP were prepared through a reduction of gold(III) derivatives.[30−32] From an energy dispersive spectrum (EDS), we observed Au characteristic peaks as shown in Figure 1c. The MEH-PPV solution dissolved in tetrahydrofuran (THF) was vigorously stirred and mixed with well-dispersed dodecanethiolate Au NPs in distilled water. The hydrophobic sites of MEH-PPV were attached with those of the dodecanethiolate Au NPs, resulting in the formation of MEH-PPV/Au NPs complexes. The detailed method for the synthesis of the MEH-PPV NPs, Au NPs, and their NPs complexes is discussed in the Experimental Section. The NP structure of the MEH-PPV/Au complex was confirmed through a HR-TEM image, as shown in Figure 1d−f. The diameters of the MEH-PPV/Au NPs were about 70−180 nm, as shown in Figure 1d. The diameters of the MEH-PPV/Au NPs were relatively larger than those of the MEH-PPV NPs because of the adsorption of the Au NPs (small black dots in Figure 1e,f) on and inside the MEH-PPV NP. We note that dodecanethiolate Au NPs could also be embedded inside the MEH-PPV NP because of the mixing process of the Au NPs in the MEH-PPV solution. From the magnification of the HR-TEM image of the NP complex shown in the inset of Figure 1e, we observed the fine and periodic stripe patterns of the Au NP, representing the atomic layer of the Au. We also observed that the diameters of the Au NPs were 2−4 nm and nanoscale gaps between the Au NPs existed, as shown in the inset of Figure 1e,f. Through FTIR spectra, we also confirmed that the complex nanostructure consisted of the MEH-PPV and dodecanethiolate Au NP. The FTIR spectrum of the MEH-PPV/Au NPs (solid bold curve) was compared with that of the MEH-PPV NPs (solid curve) and with that of the Au NPs (dotted curve), as shown in Figure 1g. The IR characteristic vibration peaks of the MEH-PPV material were observed at 1353 and 1598 cm^{-1}, which were assigned to the C−C stretch and C−H deformation vibration peak and the C−C ring stretch vibration peak, respectively. Three characteristic peaks at 2851, 2919, and 2952 cm^{-1} were observed in the MEH-PPV/Au NPs and Au NPs and were assigned

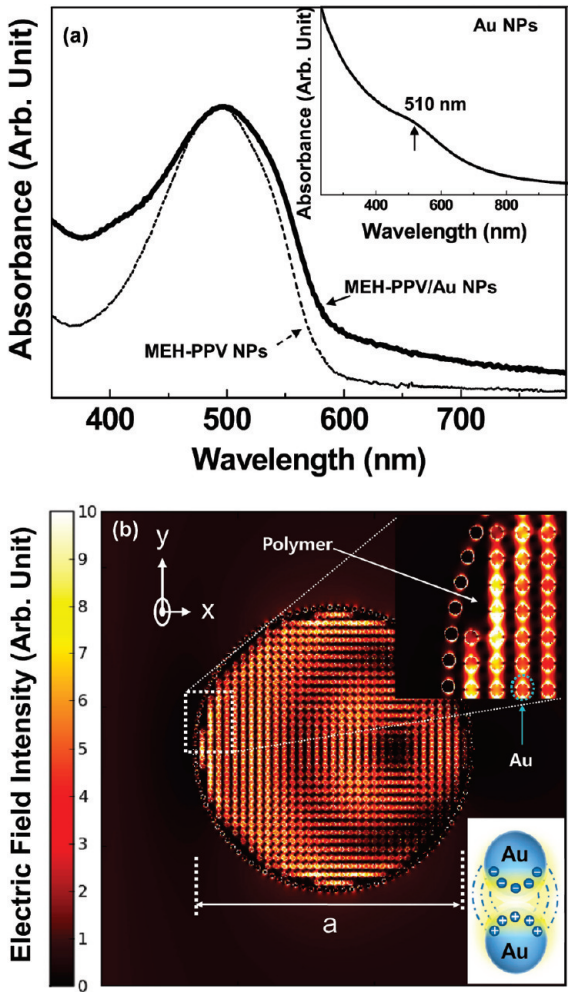

Figure 3. (a) Normalized UV−vis absorption spectra of the MEH-PPV NPs (dotted curve) and MEH-PPV/Au (solid curve) NPs in distilled water. Inset: UV−vis absorption spectrum of the Au NPs in toluene solution. (b) Local electric field distribution of the 2-D modeled nanostructure of light-emitting polymer embedded with Au, based on the FDTD calculation. Top inset: Magnification of local electric field distribution of the 2-D nanostructure of polymer/Au based on the FDTD calculation. Bottom inset: Schematic diagram of local electric field between Au spots.

to the asymmetric C−H in CH_2 due to the dodecanethiol group. A symmetric C−H bending peak in the CH_3 group at 1468 cm^{-1} appeared for the MEH-PPV/Au NPs and Au NPs due to dodecanethiol group, but that peak was not detected for the MEH-PPV NPs. From the FTIR spectra, the formation of the complex NP structure of the MEH-PPV and Au materials was confirmed.

For the study of nanoscale luminescent characteristics of an isolated single unit (*i.e.*, single particle) of the MEH-PPV and the MEH-PPV/Au NPs, LCM PL images and spectra were measured under the same experimental conditions, for example, with a focused laser power of 35 μW and a fixed excitation wavelength at 488 nm. As shown in Figure 2a,b, a three-dimensional (3-D) LCM image of the MEH-PPV/Au single NP was much brighter than that of the MEH-PPV single NP without Au NPs. The color scale bar with units of voltage on the left-hand side of Figure 2a,b represents the measured LCM PL intensity. The average of measured LCM PL intensities of the MEH-PPV/Au single NP was about 3.60 ± 0.29 V obtained from 44 different NPs, while that of the MEH-PPV single NP was about 267 ± 17.7 mV obtained from 100 different NPs. The LCM PL spectra of the single NP of the MEH-PPV and of the MEH-PPV/Au complex were compared in Figure 2c with the same acquisition time of 0.1 s. The peak intensity of the LCM PL spectrum of the MEH-PPV/Au single NP was about 30 times higher than that of the MEH-PPV single NP. We observed the LCM PL peak at about 548 and 560 nm of the MEH-PPV/Au and MEH-PPV single NP, respectively. By means of the color charge-coupled device (CCD) images shown in Figure 2d,e, we directly confirmed the increase of luminescence efficiency of the MEH-PPV NPs after the adsorption of Au NPs. The color CCD image of the MEH-PPV/Au NPs shows a relatively bright greenish-yellow light emission, in which the particle sizes (Figure 2e) seemed to be larger than the real sizes of the MEH-PPV/Au NPs because of their brightness. The enhancement of the PL efficiency of the MEH-PPV/Au NPs might have originated from the energy transfer effect in an SPR coupling.[20,21]

The SPR-assisted PL enhancement was supported by UV−vis absorbance spectra, as shown in Figure 3a. We observed the π−π* transition peaks at 490 and 495 nm for the MEH-PPV and MEH-PPV/Au NPs, respectively, as shown in Figure 3a. We also observed the UV−vis absorption peak at 510 nm for the Au NPs, representing the SP energy, as shown in the inset of Figure 3a. When a laser beam (λ_{ex} = 488 nm) was incident on the MEH-PPV/Au NPs, SPR coupling occurred between the Au NPs and the MEH-PPV NP because of the close match of the SP energy of the Au NPs and the photon energy (about 490 nm) of the MEH-PPV NP, which contributed to an effective energy transfer. Through the energy transfer in the SPR coupling, the number of excitons for band gap emission of the MEH-PPV NP increased,[20,21] resulting in the enhancement of PL efficiency of the MEH-PPV/Au NPs. We noted that the

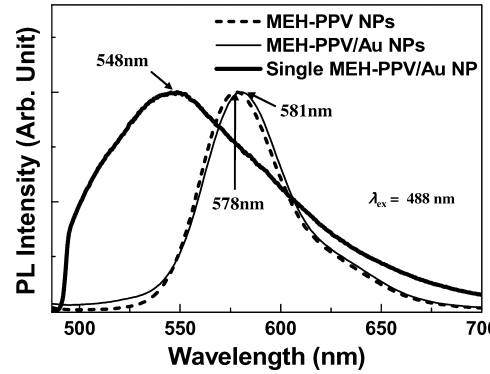

Figure 4. Comparison of normalized PL spectra of the MEH-PPV (dotted curve) and MEH-PPV/Au (solid curve) NPs in distilled water and of the single unit of MEH-PPV/Au NP complex (solid bold curve).

excitons in the MEH-PPV NPs by the incident laser beam were not quenched; rather, they contributed to the emission by energy transfer. Another important origin of the increase in luminescence efficiency might be due to a local EM field enhancement of nanogaps between the Au NPs in the background of a light-emitting MEH-PPV NP. Figure 3b shows the simulation result of a finite difference time domain (FDTD) calculation for the local EM field enhancement using the simplified nanostructures.[33] Rather than randomly distributed Au NPs on and inside a light-emitting polymer NP, we have modeled the nanostructure as a two-dimensional (2-D) cross section of an infinitely long polymer nanowire (NW) regularly embedded with Au NWs, as shown in Figure 3b. In the 2-D modeled nanostructure FDTD calculation, the diameters of the polymer and Au materials were 200 and 3 nm, respectively. The distance between Au spots was 3 nm. The incident wave was a plane wave of 488 nm. The wave propagates in the *x*-direction, and the direction of the electric field is the *y*-axis. The dielectric constants of the polymer and Au were $\varepsilon_{polymer} = 3.4225$ and $\varepsilon_{Au} = -2.214 + i3.829$ at 488 nm, respectively. The FDTD simulation results showed a strong local electric field enhancement in nanogaps between Au spots in the background of the light-emitting polymer, represented by the white and yellow parts in Figure 3b and its inset. This might also contribute to the enhancement of PL efficiency for the MEH-PPV/Au NPs.

Figure 4 shows the normalized PL spectra for a single unit and ensemble of MEH-PPV/Au NPs. For the solution PL spectrum, the MEH-PPV and MEH-PPV/Au NPs were homogeneously dispersed in distilled water. The solution PL peaks of the MEH-PPV and MEH-PPV/Au NPs were observed at 578 and 581 nm, respectively. The normalized LCM PL peaks of a single unit of the MEH-PPV and MEH-PPV/Au NPs were observed at 560 and 548 nm, respectively, as shown in Figure 2c. Compared to the solution PL spectra of the MEH-PPV and MEH-PPV/Au NPs, the solid LCM PL peaks of an isolated single unit of the MEH-PPV and MEH-PPV NPs were blue-shifted. These results might have originated from the oxidation of the single NP of the MEH-PPV and MEH-PPV/Au materials in an atmosphere.[34]

CONCLUSION

We fabricated complex NPs using a light-emitting MEH-PPV NP adsorbed with Au NPs through a reprecipitation method. The formation of the MEH-PPV/Au NP complexes was confirmed through HR-TEM and FTIR experiments. From the LCM PL images and spectra, the luminescence efficiency of an isolated single unit of the MEH-PPV/Au NPs increased considerably compared to that of a MEH-PPV single NP without the adsorption of Au NPs, which was directly confirmed through color CCD images. The enhancement of luminescence efficiency of the MEH-PPV/Au NPs might have originated from the energy transfer effect in the SPR coupling and/or the strong local field enhancement of the nanoscale gaps between Au NPs in the background of a light-emitting MEH-PPV NP supported by the FDTD simulation results. We also observed that the PL peaks of a single unit of the MEH-PPV and MEH-PPV/Au NP complex were blue-shifted, as compared with the solution PL peaks of the NPs.

EXPERIMENTAL SECTION

Materials. The NPs of poly(2-methoxy-5-(2′-ethylhexyloxy)-*p*-phenylene vinylene) (MEH-PPV) were made using a reprecipitation method.[29] The MEH-PPV (average M_n = 40 000−70 000) material was purchased from Aldrich, Inc. and used without further purification. The MEH-PPV powder was dissolved in tetrahydrofuran (THF) solution with a concentration of 1 mg/mL at room temperature (rt). The MEH-PPV solution dissolved in THF was rapidly dropped in vigorously stirring distilled water at rt. This solution was stirred for 20−30 min and then ultrasonicated for 20−30 min. The hydrophobic MEH-PPV was self-assembled into a form of NPs in distilled water. We obtained the MEH-PPV NPs after drying for 2 h on a substrate in a vacuum oven at rt. Dodecanethiolate Au NPs with a diameter of 2−4 nm were made using a reduction of gold(III) derivatives at rt based on a conventional method reported by Turkevitch.[30] The functionalized Au NPs with a dodecanethiol group were fabricated using the Brust method.[31] $AuC1_4^-$ was transferred from aqueous solution to toluene using tetraoctylammonium bromide ($C_{32}H_{68}BrN$) as the phase-transfer reagent and reduced with aqueous sodium borohydride ($NaBH_4$) in the presence of dodecanethiol ($C_{12}H_{25}SH$).[30−32] The reduced Au NPs were ultrasonicated in distilled water for 30 min at rt, and the dodecanethiolate Au NP suspension was obtained. The chemicals $HAuCl_4$, $C_{32}H_{68}BrN$, and $NaBH_4$ were purchased from Aldrich, Inc. In order to fabricate the MEH-PPV/Au NPs complexes, the MEH-PPV solution dissolved in THF was rapidly injected into a solution of Au NPs homogeneously dispersed in distilled water at rt. The suspension of MEH-PPV and Au NPs was robustly stirred for 20−30 min and then ultrasonicated for 20−30 min. The MEH-PPV/Au NP suspension was dried for 2 h on a substrate in a vacuum oven at rt. Finally, we obtained the MEH-PPV/Au NPs.

Measurements. The PL images and spectra of a single unit of the MEH-PPV and MEH-PPV/Au NPs in the nanoscale were measured by using a homemade laser confocal microscope (LCM) at rt. For the LCM PL excitation, the unpolarized argon ion laser (λ_{ex} = 488 nm) was used. In order to obtain the results shown in Figure 2, the laser power and acquisition time incident on the sample for the LCM PL measurements were fixed at 35 μW and 0.1 s, respectively. Additional details for the LCM experiment were reported previously.[20,21] We visualized the formation of the NPs using a field emission scanning electron microscope (FE-SEM, JEOL KSM-5200) and a high-resolution transmission electron microscope (HR-TEM, JEOL JEM-3010). Ultraviolet and visible absorption (UV−vis, HP-8453) and the solution PL (Aminco. Bowman FA-256) spectra were measured for the optical properties of the MEH-PPV and MEH-PPV/Au NPs, which were homogeneously dispersed in distilled water at rt. For the structural properties of the NPs, the FTIR spectra were measured using a Perkin-Elmer Spectrum GX1.

Acknowledgment. This work was supported by a Korea Science and Engineering Foundation (KOSEF) grant funded by the Korean government (MEST) (No. R0A-2007-000-20053-0). J.K. was supported by the Nano R&D program (KOSEF) funded by the MEST (No. 2008-03595).

Supporting Information Available: FDTD simulation picture of the electromagnetic wave propagation image in the 2-D polymer/Au nanostructure. This material is available free of charge *via* the Internet at http://pubs.acs.org.

REFERENCES AND NOTES

1. Zhang, H.; Wang, D.; Butler, R.; Campbell, N. L.; Long, J.; Tan, B.; Duncalf, D. J.; Foster, A. J.; Hopkinson, A.; Taylor, D.; Angus, D.; Cooper, A. I.; Rannard, S. P. Formation and Enhanced Biocidal Activity of Water-Dispersable Organic Nanoparticles. *Nat. Nanotechnol.* **2008**, *3*, 506–511.
2. Jin, R.; Cao, Y. W.; Mirkin, C. A.; Kelly, K. L.; Schatz, G. C.; Zheng, J. G. Photoinduced Conversion of Silver Nanospheres to Nanoprisms. *Science* **2001**, *294*, 1901–1903.
3. Nam, J.-M.; Thaxton, C. S.; Mirkin, C. A. Nanoparticle-Based Bio-Bar Codes for the Ultrasensitive Detection of Proteins. *Science* **2003**, *301*, 1884–1886.
4. Vaskevich, A.; Rubinstein, I. In *Handbook of Biosensors and Biochips*; Marks, R., Cullen, D., Lowe, C., Weetall, H. H., Karube, I., Eds.; Wiley: Chichester, 2007; Vol. 1.
5. Hutter, E.; Fendler, J. H. Exploitation of Localized Surface Plasmon Resonance. *Adv. Mater.* **2004**, *16*, 1685–1706.
6. Fang, Y.; Seong, N.-H.; Dlott, D. D. Measurement of the Distribution of Site Enhancements in Surface-Enhanced Raman Scattering. *Science* **2008**, *321*, 388–392.
7. Sun, Y.; Rogers, J. A. Inorganic Semiconductors for Flexible Electronics. *Adv. Mater.* **2007**, *19*, 1897–1916.
8. Ho, P. K. H.; Thomas, D. S.; Friend, R. H.; Tessler, N. All-Polymer Optoelectronic Devices. *Science* **1999**, *285*, 233–236.
9. Zhu, M.-Q.; Zhu, L.; Han, J. J.; Wu, W.; Hurst, J. K.; Li, A. D. Q. Spiropyran-Based Photochromic Polymer Nanoparticles with Optically Switchable Luminescence. *J. Am. Chem. Soc.* **2006**, *128*, 4303–4309.
10. Sun, Y.-P.; Zhou, B.; Lin, Y.; Wang, W.; Fernando, K. A. S.; Pathak, P.; Meziani, M. J.; Harruff, B. A.; Wang, X.; Wang, H.; Luo, P. G.; Yang, H.; Kose, M. E.; Chen, B.; Veca, L.; Xie, S.-Y. Quantum-Sized Carbon Dots for Bright and Colorful Photoluminescence. *J. Am. Chem. Soc.* **2006**, *128*, 7756–7757.
11. Min, Y.; Akbulut, M.; Kristiansen, K.; Golan, Y.; Israelachvili, J. The Role of Interparticle and External Forces in Nanoparticle Assembly. *Nat. Mater.* **2008**, *7*, 527–538.
12. Govorov, A. O.; Bryant, G. W.; Zhang, W.; Skeini, T.; Lee, J.; Kotov, N. A.; Slocik, J. M.; Naik, R. R. Exciton−Plasmon Interaction and Hybrid Excitons in Semiconductor−Metal Nanoparticle Assemblies. *Nano Lett.* **2006**, *6*, 984–994.
13. Kang, Y.; Taton, T. A. Controlling Shell Thickness in Core−Shell Gold Nanoparticles *via* Surface-Templated Adsorption of Block Copolymer Surfactants. *Macromolecules* **2005**, *38*, 6115–6121.
14. Tamai, T.; Watanabe, M.; Hatanaka, Y.; Tsujiwaki, H.; Nishioka, N.; Matsukawa, K. Formation of Metal Nanoparticles on the Surface of Polymer Particles Incorporating Polysilane by UV Irradiation. *Langmuir* **2008**, *24*, 14203–14208.
15. Huynh, W. U.; Dittmer, J. J.; Alivisatos, P. Hybrid Nanorod−Polymer Solar Cells. *Science* **2002**, *295*, 2425–2427.
16. Bronstein, L. M.; Valetsky, P. M.; Antonietti, M. In *Nanoparticles and Nanostructures Films. Preparation, Characterisation and Applications*; Fendler, J., Ed.; Wiley-VCH: Weinheim, Germany, 1998.
17. Schneider, G.; Decher, G.; Nerambourg, N.; Praho, R.; Werts, M. H. V.; Blanchard-Desce, M. Distance-Dependent Fluorescence Quenching on Gold Nanoparticles Ensheathed with Layer-by-Layer Assembled Polyelectrolytes. *Nano Lett.* **2006**, *6*, 530–536.
18. Kneipp, K.; Kneipp, H. SERS Signals at the Anti Stokes Side of the Excitation Laser in Extremely High Local Optical Fields of Silver and Gold Nanoclusters. *Faraday Discuss.* **2006**, *132*, 9–26.
19. Goldenberg, L. M.; Sakhno, O. V.; Smirnova, T. N.; Helliwell, P.; Chechik, V.; Stumpe, J. Holographic Composites with Gold Nanoparticles: Nanoparticles Promote Polymer Segregation. *Chem. Mater.* **2008**, *20*, 4619–4627.
20. Joo, J.; Park, D. H.; Jeong, M.-Y.; Lee, Y. B.; Kim, H. S.; Choi, W. J.; Park, Q.-H.; Kim, H. J.; Kim, D. C.; Kim, J. Bright Light Emission of a Single Polythiophene Nanotube Strand with a Nanometer-Scale Metal Coating. *Adv. Mater.* **2007**, *19*, 2824–2829.
21. Park, D. H.; Kim, H. S.; Jeong, M.-Y.; Lee, Y. B.; Kim, H. J.; Kim, D. C.; Kim, J.; Joo, J. Significantly Enhanced Photoluminescence of Doped Polymer-Metal Hybrid Nanotubes. *Adv. Funct. Mater.* **2008**, *18*, 2526–2534.
22. Ray, K.; Badugu, R.; Lakowicz, J. R. Metal-Enhanced Fluorescence from CdTe Nanocrystals: A Single-Molecule Fluorescence Study. *J. Am. Chem. Soc.* **2006**, *128*, 8998–8999.
23. Mackowski, S.; Wrmke, S.; Maier, A. J.; Brotosudarmo, T. H. P.; Harutyunyan, H.; Hartschuh, A.; Govorov, A. O.; Scheer, H.; Bruchle, C. Metal-Enhanced Fluorescence of Chlorophylls in Single Light-Harvesting Complexes. *Nano Lett.* **2008**, *8*, 558–564.
24. Anger, P.; Bharadwaj, P.; Novotny, L. Enhancement and Quenching of Single-Molecule Fluorescence. *Phys. Rev. Lett.* **2006**, *96*, 113002.
25. Anker, J. N.; Hall, W. P.; Lyandres, O.; Shah, N. C.; Zhao, J.; Van Duyne, R. P. Biosensing with Plasmonic Nanosensors. *Nat. Mater.* **2008**, *7*, 442–453.
26. Willets, K. A.; Van Duyne, R. P. Localized Surface Plasmon Resonance Spectroscopy and Sensing. *Annu. Rev. Phys. Chem.* **2007**, *58*, 267–297.
27. Schuck, P. J.; Fromm, D. P.; Sundaramurthy, A.; Kino, G. S.; Moerner, W. E. Improving the Mismatch between Light and Nanoscale Objects with Gold Bowtie Nanoantennas. *Phys. Rev. Lett.* **2005**, *94*, 017402.
28. Genet, C.; Ebbesen, T. W. Light in Tiny Holes. *Nature* **2007**, *445*, 39–46.
29. Kong, F.; Sun, Y. M.; Yuan, R. K. Enhanced Resonance Energy Transfer from PVK to MEH-PPV in Nanoparticles. *Nanotechnology* **2007**, *18*, 265707.
30. Turkevitch, J.; Stevenson, P. C.; Hillier, J. N. A Study of the Nucleation and Growth Processes in the Synthesis of Colloidal Gold. *Discuss. Faraday Soc.* **1951**, *11*, 55–75.
31. Brust, M.; Walker, M.; Bethell, D.; Schiffrin, D. J.; Whyman, R. J. Synthesis of Thiol-Derivatised Gold Nanoparticles in a Two-Phase Liquid−Liquid System. *J. Chem. Soc., Chem. Commun.* **1994**, 801–802.
32. Daniel, M.-C.; Astruc, D. Gold Nanoparticles: Assembly, Supramolecular Chemistry, Quantum-Size-Related Properties, and Applications toward Biology, Catalysis, and Nanotechnology. *Chem. Rev.* **2004**, *104*, 293–346.
33. Teflove, A.; Hagness, S. C. *Computational Electrodynamics: The Finite-Difference Time-Domain Method*; Artech House Inc.: Boston, MA, 2005.
34. Liu, C.; Kwon, Y. K.; Heo, J. Laser-Induced Blue-Shift of the Photoluminescence from PbS Quantum Dots in Glasses. *Chem. Phys. Lett.* **2008**, *452*, 281–284.